Tailoring the near-field guiding properties of magnetic metamaterials with two resonant elements per unit cell

O. Sydoruk
Department of Physics, University of Osnabrück, D-49069 Osnabrück, Germany

A. Radkovskaya
Magnetism Division, Faculty of Physics, M. V. Lomonosov Moscow State University, Leninskie Gory, Moscow 119992, Russia

O. Zhuromskyy and E. Shamonina*
Department of Physics, University of Osnabrück, D-49069 Osnabrück, Germany

M. Shamonin
Department of Electrical Engineering and Information Technology, University of Applied Sciences, D-93025 Regensburg, Germany

C. J. Stevens, G. Faulkner, and D. J. Edwards
Department of Engineering Science, University of Oxford, Parks Road, OX1 3PJ Oxford, United Kingdom

L. Solymar
Optical and Semiconductor Devices Group, Electrical and Electronic Engineering (EEE) Department, Imperial College, Exhibition Road, London SW7 2BT, United Kingdom

(Received 15 March 2006; revised manuscript received 5 May 2006; published 5 June 2006)

A theoretical and experimental study of magnetic metamaterials with unit cells containing two resonant elements is presented. The properties of these structures, consisting of split rings, are governed by strongly anisotropic magnetic coupling between individual elements. This coupling leads to propagation of slow magnetoinductive waves in the vicinity of the resonant frequency. The wavelength of magnetoinductive waves is much smaller than the free-space wavelength of the electromagnetic radiation. This opens up the possibility of manipulating the near field on a subwavelength scale. We develop a theoretical formulation for coupled chains of metamaterial elements allowing the tailoring of their guiding properties in the near field. In a comprehensive analysis modes of coupled waveguides supporting forward and/or backward waves are identified and the corresponding hybridization mechanisms for dispersion equations of magnetoinductive waves are determined. Analytical predictions are verified both experimentally and numerically on a variety of coupled waveguides. The approach can be employed for the design of near-field manipulating devices.

DOI: 10.1103/PhysRevB.73.224406 PACS number(s): 76.20.+q, 81.05.Zx, 41.20.−q, 84.30.Bv

I. INTRODUCTION

It has been known for a long time, at least for a century, that the electrical properties of a material can be influenced by inserting into it a variety of elements in a periodic or in a random manner. The recent upsurge of interest in this field is due to the recognition that those electrical properties may radically change when the elements have a resonant character. Two examples of such elements are the metallic rod of Rotman[1] and the split ring resonator of Hardy and Whitehead,[2] the former one based on linear currents and electrical interaction, and the latter one on circulating currents and magnetic interactions. Their chief merit is that they exhibit resonances with physical dimensions much smaller than the electromagnetic wavelength. The impetus for further research came from three important developments: a proof by Smith *et al.*[3] that a combination of those elements may lead to the realization of Veselago's negative index material,[4] secondly the proof of negative refraction by Shelby *et al.*,[5] and thirdly Pendry's proposal that a slab of negative index material[6] may produce subwavelength images.

Another strand of research, unrelated to the aspect of changing material properties, was concerned with the propagation of waves along resonant elements. Dispersion equations were derived by Atabekov[7] and Silin and Sazonov[8] with applications to electric filters and to slow wave structures in mind. An antenna array excited by a single element was shown to be able to support a leaky wave[9] which is partially guided and partially radiating. A physical realization of such an array of resonant elements became available in the late 1990s due to the technological advances in producing features on the nanometer scale. Tiny spheres of resonant metallic elements were produced and shown[10] to be able to support waves. Wave propagation both by transverse and longitudinal electric dipoles was demonstrated at optical wavelengths.[11,12] A similar theoretical analysis for waves along an array of loaded, electrically coupled metallic rods was carried out by Tretyakov and Viitanen.[13] In photonic crystals the possibility of guiding a wave within an impurity band by chains of coupled resonators was demonstrated by Stefanou and Modinos.[14] An optical waveguide based on similar principles was proposed by Yariv *et al.*[15] who had in mind coupling between individual defect cavities but they also considered microdisc cavities as the resonators. Taking coupling between dipoles into account Thomas *et al.*[16] considered the transfer of optical excitation energy between a

pair of identical quantum dots. Gay-Balmaz and Martin[17] observed that electromagnetic properties of individual and coupled split ring resonators differ.

It was a triumph of effective medium theory that it was capable of explaining negative refraction in a medium consisting of rods and split ring resonators. However, such a theory, based on averaging, is bound to disregard waves which may travel on the same elements. In other words effective medium theory can predict what happens to a transverse electromagnetic wave when it enters such a medium but not the waves whose existence is entirely due to those elements. Taking as examples metamaterials consisting of capacitively loaded loops, Swiss Rolls, and split ring resonators it was proven in a series of publications (see, e.g., Refs. 18–22) both theoretically and experimentally that waves, called magnetoinductive (MI) waves in this context, can indeed travel along such structures. It was also shown that these arrays may provide the basis for a variety of near-field manipulating devices[23–29] including waveguide components, transducers, and near-field imagers. In analogy to magnetoinductive waves new kind of waves, electroinductive waves,[30] have been shown to propagate on the so-called complementary metamaterials, obtained by inversion of the constituent materials with metal being replaced by the dielectric, and vice versa.

The distinguishing features of the magnetoinductive waveguide are that it works in a narrow frequency region close to the resonant frequency of the constituent elements, that it can support waves that are much slower than light, and it can work in the MHz region. Therefore we can expect that in some special applications (e.g., a radio frequency magnetic guide tuned to nuclear magnetic resonance for magnetic resonance imaging) they could replace the traditional coaxial waveguides. In this and in other applications the lack of a continuous metal path in the waveguide may be a considerable advantage when heat loss (in cryogenic applications) or the excitation of eddy currents are to be avoided.

In practice, when a device is to be designed it is essential to have considerable freedom in choosing the dispersion properties of the structure. The first successful attempt in tailoring the dispersion characteristics of MI waves[31] was based on the analogy between MI waves and phonons in solids. In a "biatomic" metamaterial chain with two elements per unit cell the dispersion curve splits into two branches, an "acoustic" and an "optical" one, separated by a band gap. Theoretical predictions were soon verified experimentally.[32] A biatomic chain of metamaterial elements may be employed as a near-field waveguide providing two distinct pass bands. A particular application may be in magnetic resonance imaging[33] when the image is required at two different frequencies far from each other. Another set of potential applications is for nonlinear MI wave interaction, e.g., for parametric amplification.[31] A similar idea was used in Ref. 34 to create a double-band metamaterial.

The new pass band in a biatomic chain of metamaterial elements is a direct consequence of biperiodicity well known in solid state physics, see, e.g., Ref. 35. It may, therefore, be expected that more complex biatomic metamaterial structures will follow similar trends and will give us additional flexibility in design. The obvious candidates are coupled chains of metamaterial elements. Couplers made of metamaterial elements were recently reported in a series of publications.[36–39] The usual analysis of two coupled lines proceeds by finding the propagation coefficients of the two unperturbed lines and then characterizing the interaction between the lines by a coupling coefficient.

The aim of the present paper is to provide a comprehensive study of the properties of two coupled chains of metamaterial elements supporting MI waves. Due to the discreteness of the metamaterial structure the overall coupling strength between the chains is determined by an interplay of a number of magnetic coupling coefficients between individual elements. In Sec. II the anisotropy of magnetic coupling coefficients is analyzed. A mathematical model is presented in Sec. III, where we derive the coupled wave equations for two one-dimensional lines of metamaterial elements. Modes of coupled guides supporting forward and/or backward waves are identified and the corresponding hybridization mechanisms for dispersion equations of MI waves are determined. Experimental results verifying theoretical predictions are presented in Sec. IV, practical implications are discussed in Sec. V, and conclusions are drawn in Sec. VI.

II. ANISOTROPY OF THE NEAR-FIELD MAGNETIC COUPLING

We consider magnetic metamaterial structures made up of resonant elements of the split ring type with both the dimensions of individual elements and the distances between them much smaller than the wavelength (the "true metamaterial limit").[40] In this case the elements can be seen as LCR circuits and can be modeled as filament circular currents. The coupling constant between two metamaterial elements depends on their relative position and orientation and is defined as follows:

$$\kappa = \frac{2M}{L} \tag{1}$$

with M being the mutual inductance and L the self-inductance of the elements. The mechanism of the magnetic coupling is that the ac current flowing in an element induces a magnetic field, which threads the neighboring element and excites a current in it. An expression for the mutual inductance based on the vector potential[41] can be obtained in the form of elliptic functions. We distinguish two cases with normals to the elements being parallel [Fig. 1(a)] and perpendicular [Fig. 1(b)] to each other. In both cases, the relative position of the second element can be described by two variables, the "lateral" shift in the plane of the first element, Δ, and the "vertical" shift in the direction of the normal of the first element, h.

Figure 1(a) shows the variation of the coupling strength with the relative position of two elements of radius r_0 with normals parallel to each other (both normals directed upwards) and Fig. 1(b) with normals perpendicular to each other (with the normal of the first element directed upwards and the normal of the second element directed to the right). Figure 1(a) contains a number of known limiting cases. If $\Delta=0$ then the elements are in the so-called *axial* configura-

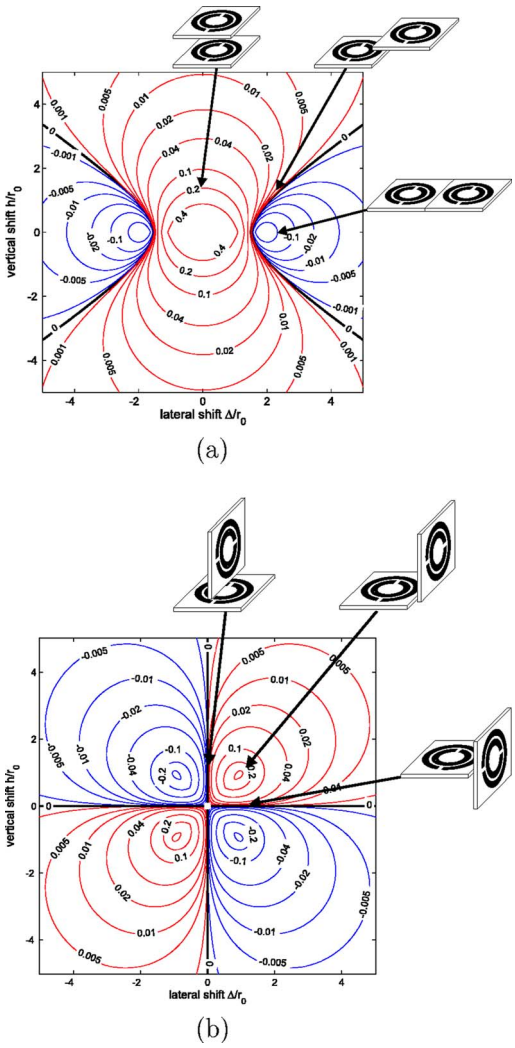

FIG. 1. (Color online) Anisotropy of the magnetic coupling between two elements. The contour plot for the coupling constant versus lateral and vertical shift. (a) With elements lying in parallel planes and (b) with elements lying in perpendicular planes.

tion, and the coupling is positive. If $h=0$ then the elements are in the *planar* configuration with negative coupling. The reason is that the magnetic field threading two neighboring elements is in the same direction for the axial case and in the opposite direction for the planar case. The coupling constant is identical for all four quadrants of the plane (Δ,h) so it is sufficient to discuss the properties of the first quadrant $\Delta \geqslant 0$, $h \geqslant 0$. There is a curve of zero coupling on the plane (Δ,h). For any set of (Δ,h) above this curve the coupling is positive, and for any set of (Δ,h) below the curve it is negative. The situation is quite different [Fig. 1(b)] when the normals of the elements are perpendicular to each other. The limiting cases are as follows: there is no coupling if either of the shifts is zero, $\Delta=0$ or $h=0$, which follows from a symmetry argument. The coupling is positive for the first and third quadrants and negative for the second and fourth quadrants.

Note that the coupling constant is real as long as the distance between the elements is much smaller than the wavelength of the electromagnetic wave. If the size of the elements and/or the distance between them become comparable with the wavelength of the electromagnetic wave, retardation effects may become important and the coupling constant may become complex.[22] In the following we shall make use of the anisotropy of the magnetic coupling in constructing a variety of structures carrying magnetoinductive waves with distinct dispersion relations.

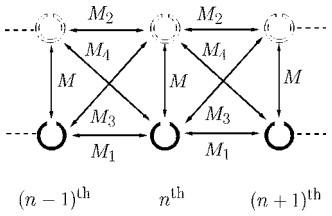

FIG. 2. Schematic presentation of the coupling between two lines of resonant magnetic metamaterial elements. Mutual inductances M_1, M_2, M, M_3, and M_4 between the nearest neighbors are shown by arrows.

III. THEORY OF COUPLED MODES FOR MI WAVES

A. General formulation

We shall analyze the interaction mechanisms between two chains of resonant metamaterial elements with magnetic coupling between nearest neighbors. The derivation presented here can easily be generalized to the case of couplings between any pair of elements. However, as shown in Sec. II the mutual inductances between the elements decline fast and it may be justified (at least in the pass bands) to take only nearest neighbor interactions into account. We shall return to the problem of many-element interactions in Sec. IV.

We start with an equidistant linear array of identical resonant elements coupled magnetically to their nearest neighbors. Kirchhoff's voltage equation for the nth element is of the form

$$Z_{01}I_n + Z_1(I_{n-1} + I_{n+1}) = V_n^{(1)}, \tag{2}$$

where harmonically varying signals of frequency ω are assumed. Here Z_{01} is the complex self-impedance of each one of the elements. Z_1 is the pure imaginary mutual impedance between the neighboring elements, I_n is the current in, and $V_n^{(1)}$ is the voltage applied to the nth element.

Let us now consider a second linear array. Kirchhoff's equation may similarly be written as follows:

$$Z_{02}J_n + Z_2(J_{n-1} + J_{n+1}) = V_n^{(2)}, \tag{3}$$

where subscript 1 has now been replaced by subscript 2 and the current in the nth element is denoted by J_n. The complex self-impedance of elements of each line has the form $Z_{0i} = R_i + j\omega L_i + 1/(j\omega C_i)$ with resistance R_i, self-inductance L_i, and capacitance C_i $(i=1,2)$. The purely imaginary mutual impedance Z_i is equal to $j\omega$ times the mutual inductance M_i.

If the lines are close enough to each other their elements are coupled not only to the elements of their own lines but also to the elements of the other line. As may be seen in Fig. 2 a general element in the line is coupled to its five neighbors

by the mutual inductances M_1, M_2, M, M_3, and M_4. The additional mutual inductances are M, the mutual inductance within the unit cell, M_3, the mutual inductance between the nth element of line 1 and the $(n+1)^{\text{th}}$ element of line 2, and M_4, the mutual inductance between the nth element of line 2 and the $(n+1)^{\text{th}}$ element of line 1. Kirchhoff's equations must then be modified by adding the interaction terms due to mutual impedances $Z=j\omega M$, $Z_3=j\omega M_3$, and $Z_4=j\omega M_4$ to the left-hand side (LHS) of Eqs. (2) and (3) yielding

$$Z_{01}I_n + Z_1(I_{n-1} + I_{n+1}) + ZJ_n + Z_4J_{n-1} + Z_3J_{n+1} = V_n^{(1)},$$

$$Z_{02}J_n + Z_2(J_{n-1} + J_{n+1}) + ZI_n + Z_3I_{n-1} + Z_4I_{n+1} = V_n^{(2)}. \quad (4)$$

Two coupled lines can be considered as a biatomic chain of metamaterial elements with the unit cell containing two elements with the currents I_n and J_n in the upper and lower lines, respectively.

Our next aim is to find the dispersion equation, i.e., to relate the frequency ω to the wave number k. In the presence of losses k is complex and can be written in the form $k=\beta - j\alpha$ where β and α are the propagation and attenuation constants, respectively. We may then disregard the applied voltages and look for wave solutions in the form $I_n = I_0 \exp[j(\omega t - nkd)]$ and $J_n = J_0 \exp[j(\omega t - nkd)]$, where I_0 and J_0 are constants, ω is the frequency, and d is the period of the lines. Equations (4) may then be recast in the form

$$Z_{01}I_0 + 2j\omega M_1 I_0 \cos kd + j\omega(M + M_4 e^{jkd} + M_3 e^{-jkd})J_0 = 0,$$

$$Z_{02}J_0 + 2j\omega M_2 J_0 \cos kd + j\omega(M + M_3 e^{jkd} + M_4 e^{-jkd})I_0 = 0. \quad (5)$$

Equations (5) have nontrivial solutions when the determinant of the coefficients of I_0 and J_0 vanishes yielding the relationship between ω and kd

$$(Z_{01} + 2j\omega M_1 \cos kd)(Z_{02} + 2j\omega M_2 \cos kd) = -\omega^2\sigma(kd) \quad (6)$$

with the coupling coefficient

$$\sigma(kd) = M^2 + M_3^2 + M_4^2 + 2M(M_3 + M_4)\cos kd + 2M_3M_4 \cos 2kd. \quad (7)$$

Note that we distinguish here between the coupling *coefficient* $\sigma(kd)$ in Eq. (7) characterizing the overall coupling strength between the lines and the coupling *constant* κ in Eq. (1) which determines the coupling between the individual elements.

Equation (6) is clearly in the form of coupled wave equations with $\sigma(kd)$ as the coupling coefficient. If $\sigma(kd)=0$ then the brackets on the LHS of Eq. (6) give the dispersion equations of the uncoupled lines.

Let us now briefly discuss the properties of Eq. (6). It can be solved either for ω or for kd. In terms of $\cos kd$ Eq. (6) is an algebraic equation of the second order giving two solutions. This means that there are two (in general complex) values of kd corresponding to one real value of ω. Such a situation was discussed by Brillouin.[42] For ω it is a biquadratic equation. For the lossless case (self-impedances Z_{01} and Z_{02} have no real parts) we find that, as long as $\omega^2\sigma(kd)$ is positive, real values of kd give real values of ω, leading to two passbands of the dispersion characteristics

$$\omega_{1,2} = \sqrt{\frac{\omega_{01}^2\Gamma_2 + \omega_{02}^2\Gamma_1 \pm \sqrt{(\omega_{01}^2\Gamma_2 - \omega_{02}^2\Gamma_1)^2 + 4\dfrac{\omega_{01}^2\omega_{02}^2}{L_1L_2}\sigma(kd)}}{2\left(\Gamma_1\Gamma_2 - \dfrac{1}{L_1L_2}\sigma(kd)\right)}}, \quad (8)$$

where $\omega_{0i}=1/\sqrt{L_iC_i}$ is the resonant frequency of the elements in line i and $\Gamma_i=1+(2M_i/L_i)\cos kd \equiv 1+\kappa_i \cos kd$. The subscripts 1 and 2 in Eq. (8) refer to lines 1 and 2 but note that ω_1 and ω_2 denote now the variations with frequency in passbands 1 and 2, respectively.

It may be seen from Eq. (8) that the group velocity, $d\omega/dk$, is zero at the edges of the band, at $kd=0$ and $kd=\pm\pi$ but it can also be zero within the Brillouin zone when the following equation is satisfied:

$$\frac{\left[\dfrac{j}{\omega}(M_1Z_{02} + M_2Z_{01}) + M(M_3 + M_4)\right]^2}{4(M_3M_4 - M_1M_2)} = \frac{Z_{01}Z_{02}}{\omega^2} + M^2 + (M_3 - M_4)^2. \quad (9)$$

If Eq. (9) has real solutions for ω then it must refer to either a minimum or a maximum of the dispersion curve $\omega(kd)$. The presence of such an extremum in one or both branches of the dispersion curve obviously means that the same branch may support both forward and backward waves for different ranges of kd. It is also known[43–45] that the presence of an extremum within the interval $0<kd<\pi$ will give rise to complex modes.

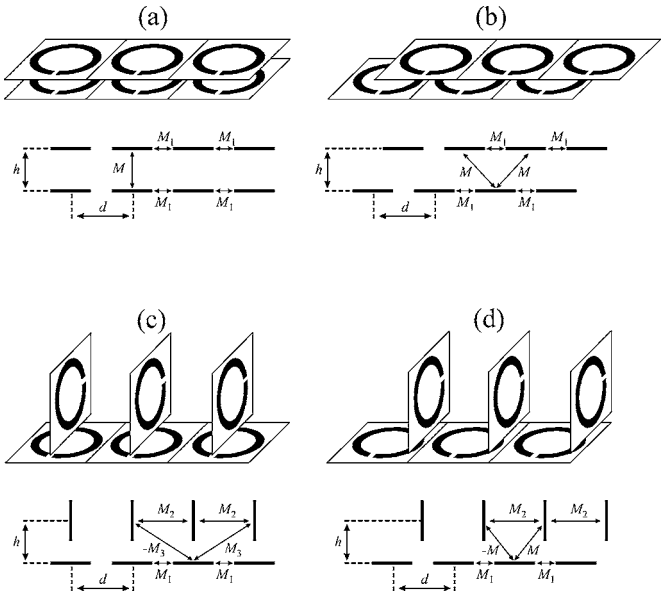

FIG. 3. Configurations of biatomic metamaterial structures with co-directional (a), (b) and contradirectional (c), (d) power flow. (a) Planar lines above each other. (b) Shifted planar lines. (c) Planar and axial line above each other. (d) Shifted planar and axial lines. The nonzero mutual inductances are shown by arrows.

In the stop bands, in the lossless case, kd is either purely imaginary or complex. Two limiting cases occur at $kd=0-j\alpha d$ and $kd=\pi-j\alpha d$. The decay is monotonic in the first case whereas the sign of the amplitude alternates in the second case. They correspond to Kelvin's evanescent waves.[42]

We shall now apply the developed theoretical formulation of coupled chains of metamaterial elements to a variety of configurations with the aim to tailor their near-field guiding properties. It is customary to put couplers into two distinct categories, co-directional and contradirectional, depending on whether the phase velocities of the two lines are in the same or in opposite directions. In our case, MI waves allow us to choose for the unperturbed lines both forward (axial configuration) and backward (planar configuration) wave propagation.[19] The freedom in choosing the relative position of both chains would lead to a great variety of mutual coupling effects and would provide an additional flexibility in tailoring the dispersion characteristics of coupled MI waves. For simplicity we shall, from now on, assume all elements to be identical, $Z_{01}=Z_{02}=Z_0$.

B. Coupled modes with co-directional and contradirectional power flow

1. Configurations

For a detailed investigation we have chosen configurations shown schematically in Fig. 3. The cases of interest are two coupled planar lines, (a) and (b), and coupled planar and axial lines, (c) and (d). The unit cell in each case consists of two elements. The elements within the unit cell are exactly above each other in cases (a) and (c) and shifted by one half of the period in cases (b) and (d). The mutual inductances, taken as different from zero, are shown in Figs. 3(a)–3(d) for all four cases.

In cases (a) and (b) both lines, if uncoupled, support backward waves. For these cases $M_1=M_2<0$. In cases (c) and (d) one line is planar and the other one is axial. For these two configurations the mutual inductances M_1 and M_2 are different having both different signs and absolute values, $M_1<0$ and $M_2>0$, so that one line supports backward and the other one forward waves.

In case (a) the identical planar lines are exactly above each other. As may be expected the mutual inductances M_3 and M_4 do not greatly influence the coupling between the lines and can therefore be neglected [see also Fig. 1(a)]. The dispersion equation (6) reduces to

$$(Z_0+2j\omega M_1\cos kd)^2=-\omega^2M^2. \tag{10a}$$

In case (b) when the two planar lines are shifted relative to each other by one half of the period $M_3=M$ for symmetry reasons while M_4 can be neglected [see also Fig. 1(a)]. The dispersion relation is

$$(Z_0+2j\omega M_1\cos kd)^2=-2\omega^2M^2(1+\cos kd). \tag{10b}$$

In case (c) the planar and the axial lines are exactly above each other. Since the planes of the loops within the unit cell are perpendicular to each other the mutual inductance within the unit cell, M, is zero so that interaction takes place via M_3 and M_4 which have equal absolute values and opposite signs, $M_4=-M_3$ [see also Fig. 1(b)]. The dispersion equation is of the form

$$(Z_0+2j\omega M_1\cos kd)(Z_0+2j\omega M_2\cos kd)=-2M_3^2\omega^2(1-\cos 2kd). \tag{10c}$$

In case (d) the planar and the axial lines are in the half-period-shifted configuration. In this case $M_3=-M$ while M_4 can be neglected [see also Fig. 1(b)]. The corresponding dispersion equation is of the form

$$(Z_0+2j\omega M_1\cos kd)(Z_0+2j\omega M_2\cos kd)=-2\omega^2M^2(1-\cos kd). \tag{10d}$$

2. Properties of the dispersion relations

We now illustrate the properties of the dispersion relations [Eqs. (10a)–(10d)] choosing as an example a set of parameters relevant to the actual realization of the elements used in our experiments. Since one of the potential applications of metamaterials is in magnetic resonance imaging (MRI), we choose $f_0=\omega_0/(2\pi)=46.2$ MHz corresponding to a magnetic field close to 1 T. The radius of the element is taken as $r_0=10$ mm. It is worth mentioning that the chosen approach of modeling the elements as resonant filament currents still leaves a considerable degree of generality and was proven to work well to describe the experimental results for a variety of metamaterial elements suitable for MRI applications including capacitively loaded metallic loops,[20] Swiss Rolls,[21,27] and capacitively loaded split pipes.[32] The latter elements shall also be employed in the experiments presented in Sec. IV. All the elements mentioned have it in

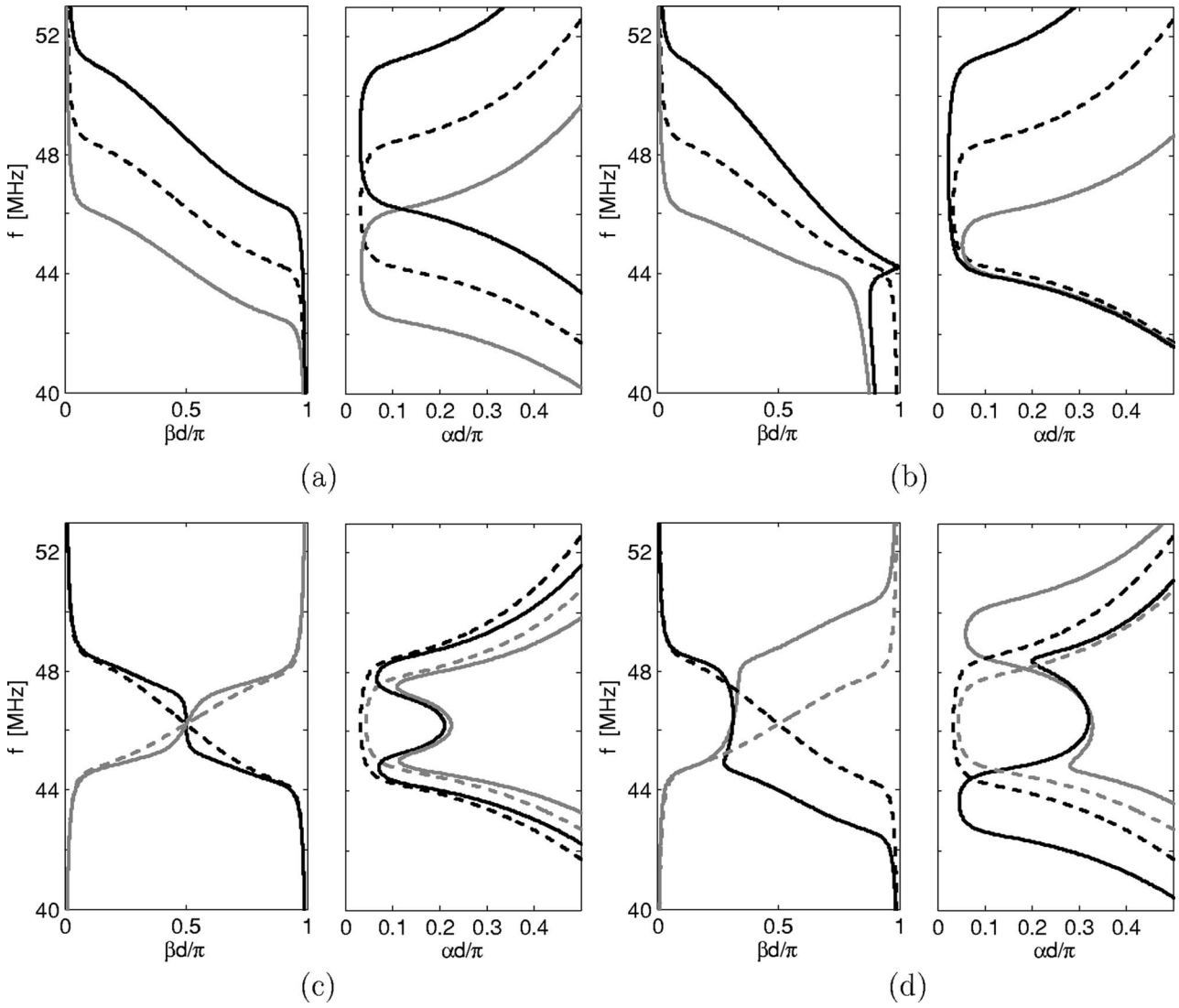

FIG. 4. Dispersion characteristics of the coupled lines of Fig. 3. Dashed lines show the unperturbed dispersion curves.

common that they are designed to work in the "true metamaterial limit"[40] as the radius of elements, about 1 cm, is 2–3 orders of magnitude smaller than the wavelength of the electromagnetic radiation of 5–15 m (corresponding to resonant frequencies of 60–20 MHz). The losses will be characterized by the elements' quality factor of $Q=105$. The stop bands are indicated by a significant increase of the attenuation constant.

For a clearer comparison of dispersion relations we choose, for all four configurations, the same period d and the same distance h between the two lines [see Figs. 3(a)–3(d)]. Note that the distance between neighboring elements within a planar line cannot be smaller than $2r_0$. We shall choose $d=24$ mm close to this minimum. The distance between the planar and the axial line cannot be smaller than r_0. We shall choose $h=15$ mm.

The dispersion equations (10a)–(10d) with propagation and attenuation constants versus frequency for the four biatomic configurations are plotted in Figs. 4(a)–4(d). The dashed lines show the dispersion equations for the unperturbed lines (with the interaction between the lines switched off, $M=M_3=M_4=0$), whereas the solid lines are for the coupled lines.

In case (a) the identical planar lines are exactly above each other. Since the lines are identical the unperturbed dispersion characteristics (dashed line) must be identical as well. The unperturbed dispersion equation describes a backward wave corresponding to the coupling constant $\kappa_1=-0.09$ with the passband given by $(1-\kappa_1)^{-1/2}=\omega/\omega_0=(1+\kappa_1)^{-1/2}$. In the presence of coupling between the lines one dispersion curve (black solid line) moves upwards, and the other one (grey solid line) downwards as may be clearly seen from Fig. 4(a). The separation in frequency between the two branches is determined by the strength of the coupling constant κ which for the chosen parameters has the value, $\kappa=0.19$. The separation in frequency remains the same for all values of βd; this conclusion follows also from the form of Eq. (10a) with the right-hand side (RHS) independent of kd. For the chosen parameters the interaction between the lines is so large that the two branches are separated by a complete stop band. It could be expected that if the distance h between the lines were larger, the interaction between the lines would

be weaker and the separation between the two branches would not result in a complete stop band between them. In such a case we would expect the behavior typical for couplers: two values of βd for a single ω leading to a beating of the two signals and consequently to a periodic exchange of power between the lines. This prediction shall be checked in Sec. IV where we discuss experimental results.

In case (b) the identical planar lines are shifted relative to each other by half a period. The unperturbed dispersion equation of course does not change, but the behavior of the dispersion equations for coupled lines changes drastically in comparison with case (a). It can be seen from the RHS of Eq. (10b) that the coupling coefficient (and consequently the interaction process) between the MI waves is now different within the Brillouin zone itself: it is maximum at $kd=0$ and entirely absent at $kd=\pi$. It may therefore be expected that the amount of split will depend on βd. This is indeed what happens as may be seen in Fig. 4(b). For the chosen parameters the coupling constants are $\kappa_1=-0.09$ and $\kappa=0.1$. The resulting two branches are very different from each other. The interaction results in an upper branch with a wider passband than in the unperturbed case (black solid line) and in a lower branch with a narrower passband (grey solid line). There is a noticeable minimum for the lowest branch. This means that forward waves may also exist for a certain range of frequency. The probable physical reason is that the mutual inductance M is positive and large enough to suppress the negative mutual inductance M_1. The position of the minimum may be obtained from Eq. (10b) as follows:

$$\frac{\omega}{\omega_0}=\left(1-\kappa_1-\frac{\kappa^2}{8\kappa_1}\right)^{-1},\quad \cos kd=\frac{\kappa^2}{8\kappa_1^2}-1. \qquad (11)$$

Below this point the propagation and attenuation constants represent the complex modes. Note that we take $|\beta d|$ so that waves propagating in the different directions are in the same half of the Brillouin zone.

In case (c) the planar and axial lines are exactly above each other. The interaction mechanism is in this case quite different from the cases of two planar lines (a) and (b). The two unperturbed dispersion curves show a backward wave for the planar line [black dashed line in Fig. 4(c)] and a forward wave for the axial line [grey dashed line in Fig. 4(c)]. These curves correspond to the coupling constants $\kappa_1=-0.09$ and $\kappa_2=0.07$. Consequently the passband of the backward wave in the planar line one is slightly wider than the passband of the forward wave in the axial line two. The unperturbed dispersion curves cross at $\beta d=\pi/2$ which can be seen to be a point of degeneracy. The interaction between the lines is governed by relatively weak coupling constants $\kappa_{3,4}=\pm 0.05$. As can be seen from Eq. (10c) the interaction is absent for $kd=0,\pi$ where the unperturbed dispersion curves are far away from each other and it is maximum for $kd=\pi/2$ at their crossing point. The resulting dispersion curves show the split of the passband into two with the stop band around the point of degeneracy. The coupled dispersion curves are quite close to the unperturbed ones except in the vicinity of the degenerate point $\beta d=\pi/2$ where complex modes of high attenuation appear. In both passbands there

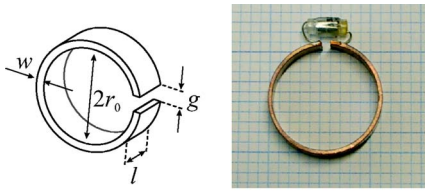

(a) (b)

FIG. 5. (Color online) Schematic presentation of the element (a), its photograph (b).

are frequency regions with two values of βd for a single ω which would result in a beating of the two signals. Contrary to case (a) with two backward waves we have here a contradirectional mode where both forward and backward waves can simultaneously propagate.

In case (d) the planar and axial lines are in the half-period-shifted configuration. The unperturbed dispersion curves [dashed lines in Fig. 4(d)] are the same as in the unshifted configuration (c). The coupling mechanism governed by the coupling constants $\kappa=-\kappa_4=0.15$ changes drastically in comparison with case (c). As may be seen from Eq. (10d) the interaction is zero for $kd=0$ and maximum for $kd=\pi$. The resulting dispersion in Fig. 4(d) shows two complex passbands supporting both forward and backward waves with the separation between the two branches increasing with βd. Another consequence of the interaction between the lines, that is different within a Brillouin zone, is that the degenerate point is not at $\beta d=\pi/2$, as in the previous case, but shifts towards smaller values of βd. The attenuation of the two modes [solid black and gray lines in Fig. 4(d)] is different within the passbands: for the lower one the backward-wave mode (black line) has lower attenuation whereas for the upper passband the forward wave dominates.

To sum up, in addition to the two classical types of hybrid modes for coupled waves on unshifted lines [cases (a) and (c)], we have also observed two novel hybrid modes for the half-period shifted lines where the interaction is strongly dependent on the propagation constant. In case (b) maximum interaction is at $kd=0$ and zero at $kd=\pi$ whereas for case (d) the points of maximum and zero interaction are reversed.

IV. EXPERIMENT

We performed a series of experiments in order to check the validity of our theoretical approach. In particular the following points were addressed:

(i) the validity of the filament-current approach used for studies of the anisotropy of the coupling coefficients;

(ii) the validity of the nearest neighbor approximation;

(iii) the verification of the different coupled modes.

A. Elements

The elements used in the experiments are capacitively loaded split pipes. A photograph may be seen in Fig. 5(b) and a schematic drawing in Fig. 5(a) showing the dimensions: inner diameter, $2r_0=20$ mm, wall thickness, $w=1$ mm, wall height, $l=5$ mm, and gap width, $g=2$ mm. They are loaded

by nominally identical capacitors of 330 pF. Their resonant frequencies and quality factors measured with the aid of a network analyzer of the type HP8753C were found as $f_0 = \omega_0/(2\pi) = 46.2 \pm 0.2$ MHz and $Q = 105 \pm 5$.

B. Coupling constant measurements

The magnetic coupling between the elements was determined by measurements on two elements only. The transmitting loop is placed close to the first element, and the receiving loop scans the magnetic field produced by the first element and by the second element. The ratio of the signals gives the ratio of currents in the elements, I_2/I_1, and is related to the coupling constant[20] as

$$\frac{2I_2}{I_1} = \kappa\left(1 - \frac{\omega^2}{\omega_0^2} - \frac{j}{Q}\right)^{-1}. \tag{12}$$

Matching the measured dependence of I_2/I_1 on frequency gives the experimental value of κ. Note that there are no other free parameters as the resonant frequency ω and the quality factor Q are known. The measured values of κ differ from the theoretical values provided by our model by less than 15% in configurations when the elements are close to each other and start to coincide for distances between the elements larger than $4r_0$.

C. Dispersion equations

We analyzed the waveguiding properties of the four biatomic metamaterial configurations (a)–(d) arranging the elements into two lines each containing 16 elements. The period d was kept to be 24 mm in all cases, for the distance h between the lines three values were chosen for each configuration, $h = 10$, 15, 20 mm for cases (a) and (b) and $h = 15$, 20, and 30 mm for cases (c) and (d). The first element of line one was excited by the transmitting loop, and the frequency dependence of the currents in all elements were measured as the receiving loop was moved first along line one and then along line two. The measurements were performed in the 1601 frequency points for the range 34–58 MHz with the aid of the same network analyzer.

To extract the dispersion equations for the coupled lines we used the following procedure. We assume that for each frequency ω the structure supports two modes with two complex values of kd. We should take into account that the structure has a finite length and that there are reflected waves as well. Then the currents in line one and line two can be written as follows:

$$I_n = a_1 \exp(-jnk_1d) + b_1 \exp(jnk_1d) + a_2 \exp(-jnk_2d) + b_2 \exp(jnk_2d),$$

$$J_n = c_1 \exp(-jnk_1d) + d_1 \exp(jnk_1d) + c_2 \exp(-jnk_2d) + d_2 \exp(jnk_2d). \tag{13}$$

k_1d and k_2d can thus be found from an algebraic expression containing values of any six neighboring currents within either line one or line two. Following a similar procedure the unperturbed dispersion equations can be found from current measurements of isolated lines. Assuming in this case a single mode and its reflected wave, the dispersion equation can be extracted from the values of any three neighboring currents of the line.

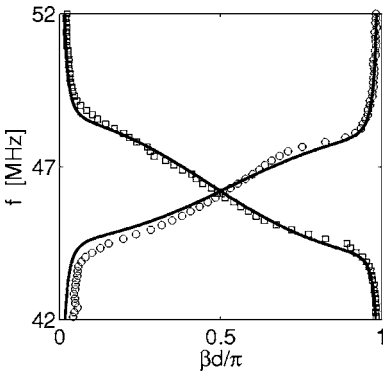

FIG. 6. Dispersion characteristics of the uncoupled planar and axial lines: theory (solid lines) and experiment (circles and squares).

Figure 6 shows the dispersion curves for the case of uncoupled lines supporting backward and forward waves. The experimental values are denoted by circles and squares and the theoretical ones by solid lines. The agreement may be seen to be excellent. Figure 7 gives a summary of the dispersion curves for each one of the coupled configurations. The first and second columns [Figs. 7(a) and 7(b)] are for $h = 20$, 15, and 10 mm for planar-planar configurations unshifted and shifted, respectively. The third and fourth columns show the dispersion curves for $h = 30$, 20, and 15 mm for planar-axial configurations, unshifted in Fig. 7(c) and shifted in Fig. 7(d). In each of the four columns the top figure corresponds to the largest separation between the lines and thus to the weakest interaction, the bottom figure corresponds to the smallest separation and thus to the strongest interaction. Comparing the figures in each column we can clearly see the different characters of the respective coupling mechanisms.

For the first column [Fig. 7(a)], when two planar lines are exactly above each other [Fig. 4(a)], the unperturbed dispersion curve splits into two similar branches; the separation between the branches grows as the distance, h, between the lines decreases.

For the second column [Fig. 7(b)], when the planar lines are half-period shifted relative to each other, the upper branch is a backward-wave branch with a wider passband, and the lower branch supports both forward and backward waves with a minimum within a Brillouin zone [Fig. 4(b)]. The separation between the branches depends strongly on the propagation constant and is maximum for $\beta d \to 0$ and minimum for $\beta d \to \pi$.

For the third column [Figs. 7(c)], when the planar and the axial line are exactly above each other [Fig. 4(c)], the interaction between a backward and a forward wave of Fig. 6 results in a stop band around the resonant frequency. The coupled dispersion curves differ from the unperturbed ones mostly in the vicinity of the crossing point $\beta d = \pi/2$. The smaller the separation between the lines, the better pronounced is the effect.

For the fourth column [Fig. 7(d)] when the planar and the axial line are half-period shifted relative to each other, the

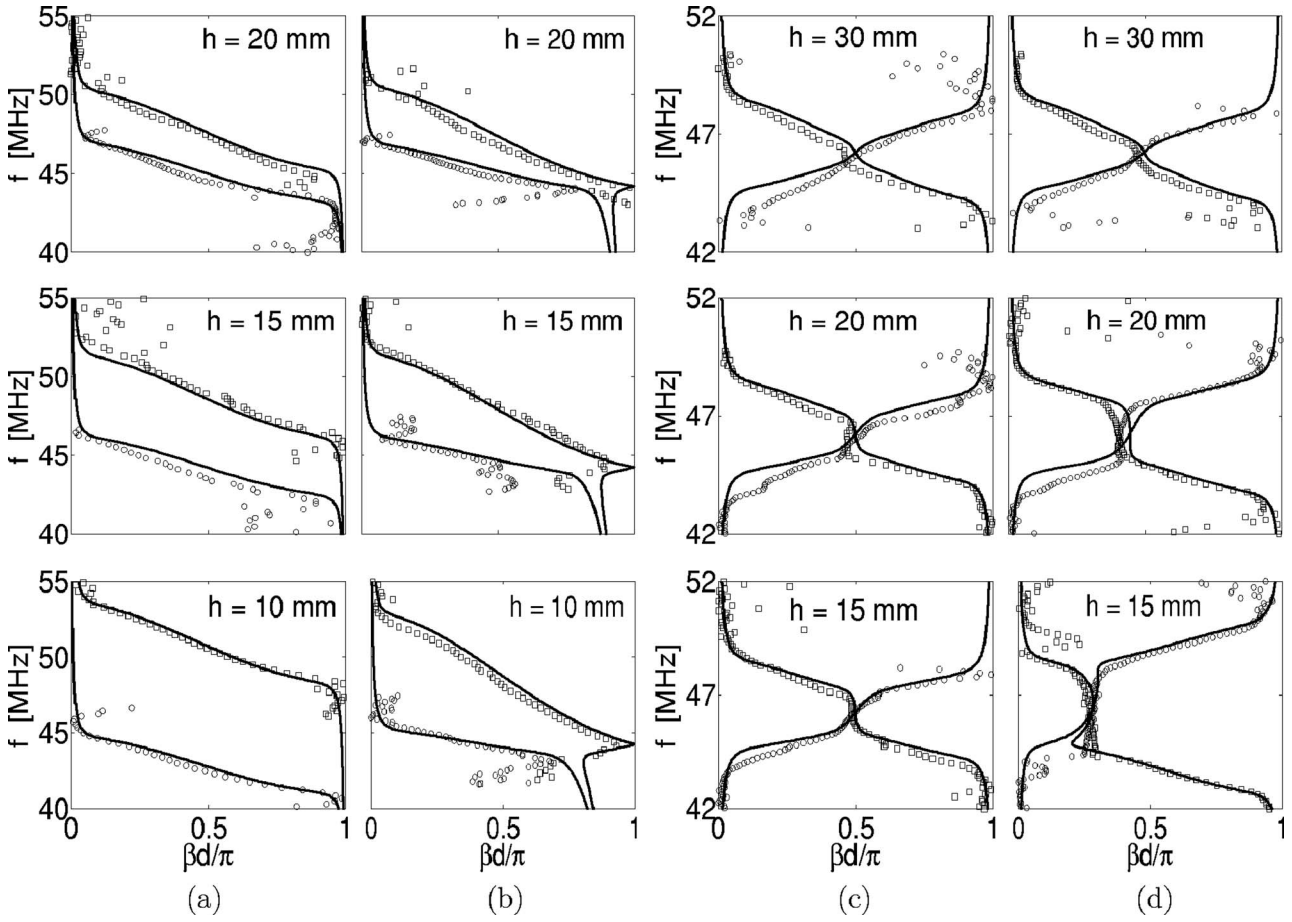

FIG. 7. Dispersion characteristics of the coupled lines: Theory (solid lines) and experiment (circles and squares). Unshifted (a) and shifted (b) planar-planar lines with $h=20,15,10$ mm. Unshifted (c) and shifted (d) planar-axial lines with $h=30,20,15$ mm.

separation between the branches depends strongly on the propagation constant [Fig. 4(d)]. The separation is maximum for $\beta d \to \pi$ and minimum for $\beta d \to 0$. The degenerate point may be seen to be around $\beta d = \pi/2$ for the distance $h = 30$ mm between the lines and it moves to the left as the distance between the lines decreases.

The agreement between theory [provided by Eqs. (10a)–(10d)] and experiment may be seen to be very good in the passbands in each one of the 12 diagrams of Fig. 7. Note that the experimental points in the stop bands had magnitudes close to the noise level due to the high attenuation so they are probably spurious.

D. Validity of nearest neighbor approximation

The theoretical curves were obtained in the approximation of nearest neighbor interactions where each element is interacting with up to five neighbors.

As an additional check of the validity of the model we also performed numerical simulations modeling the signal propagation in our structures by taking all interactions into account. Figure 8 shows an example of the power distributions along the structure for the unshifted planar-planar configuration with the separation between the lines $h=20$ mm at the frequency $f=\omega/(2\pi)=45.8$ MHz which is close to the resonant frequency of the individual element. Figures 8(a) and 8(b) show the distribution of detected power along lines one and two respectively. The squares are the experimental values, the diamonds are the values obtained from the analytical theory with nearest neighbor interactions, and the circles are the numerical simulation values from impedance matrix calculation taking all interactions into account.[21] The agreement between experiment, theory and numerical results may be seen to be good. The beating of the signals in line one and line two are in antiphase, as the energy is transferred from line one to line two and back. At the chosen frequency the two lines act as a co-directional coupler [Fig. 7(a), $h = 20$ mm], and the corresponding values of the propagation constant are [from Eq. (10a)] $\beta_1 d = 0.36\pi$ and $\beta_2 d = 0.73\pi$. The coupling length characterizing the period of energy transfer is $\Lambda = \pi/|\beta_1 - \beta_2|$. This gives the period of the energy exchange of about five elements.

A similar agreement between the calculated and measured values of current amplitudes within the structure is obtained for all configurations for frequency values corresponding to the passbands.

V. PRACTICAL IMPLICATIONS

An area of potential applications of biatomic metamaterial structures supporting magnetoinductive waves is magnetic

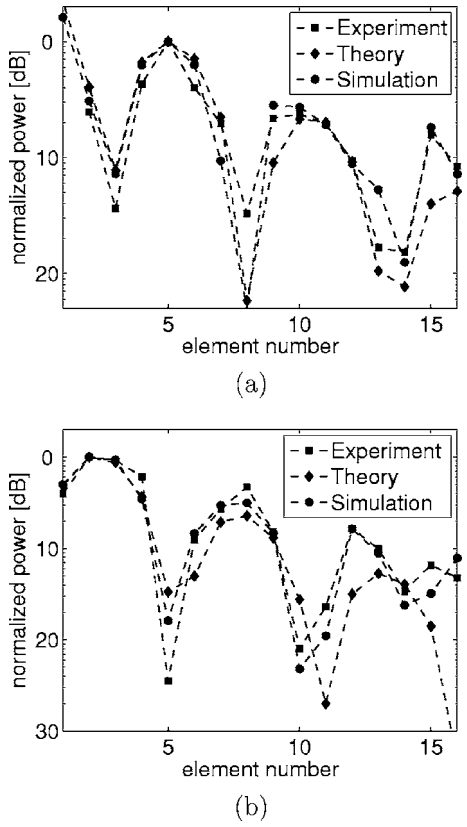

FIG. 8. Power distribution along the excited line one (a) and line two (b) for the unshifted planar-planar configuration. $h=20$ mm, $f=45.8$ MHz. Experiment (squares), analytical theory with nearest-neighbor approximation (diamonds), numerical simulation including all interactions (circles). The lines connecting the symbols serve as a guide to the eye.

resonance imaging. It is a technique where strong dc magnetic fields and weak rf magnetic fields are involved. Ferromagnetic materials are unsuitable because they would interfere with the dc magnetic field. What is needed is a material which has high magnetic response in the narrow frequency range around the magnetic resonance being nonmagnetic at dc. Magnetic metamaterials supporting magnetoinductive waves can easily satisfy these requirements. Their wavelength is much shorter than the free-space wavelength of the electromagnetic radiation, which implies that the size of the magnetoinductive wave devices is also small relative to the wavelength. For the above mentioned example of the codirectional coupler the free-space wavelength of electromagnetic radiation is about 6.6 m, whereas the full power transfer from the first (excited) to the second line takes place on a much smaller distance of 6 cm. The additional flexibility in tailoring the dispersion properties of coupled MI waves provided by biatomic metamaterial structures further improves the possibility of manipulating the magnetic fields on a subwavelength scale. Parametric amplification of magnetoinductive waves propagating in a biatomic metamaterial structure, which includes nonlinear elements, e.g., a varactor diode,[46,47] may be used for enhancing the performance of MRI devices by improving the signal-to-noise ratio.

The mechanism for near-field imaging with silver multilayered metamaterials[48] is provided by excitation of surface plasmons.[6] Regarding magnetic metamaterials, there is, however, not enough evidence at the moment to say which of various mechanisms is responsible for near-field imaging with magnetic metamaterials or whether all of them show different facets of the same physical phenomenon. Pendry's proof of "perfect imaging" was based on the fact that with a negative index material it is possible (at least in principle) to obtain a flat transfer function in the spatial frequency region.[6] An alternative explanation of imaging for the two-layer case may be based on the curvature of the dispersion characteristics as discussed for example by Zengerle,[49] Smith *et al.*,[50] Silin,[51] and Belov *et al.*[52] The explanation of imaging with a single layer of Swiss Rolls was based on the existence of a negative permeability region.[53–55] The presence of MI waves in a one-dimensional layer was shown to lead to strong distortion of the image.[27,54] When the structure consists of two parallel two-dimensional arrays of metamaterial elements then MI waves may play a positive role.[24] They may be responsible for obtaining the right current distribution on the outer array for imaging when the inner array is excited by the object. The present model of coupled modes in a biatomic metamaterial structure is potentially suitable for the design of a near-field magnetoinductive lens with required properties.

Recent developments in the field of metamaterials research when miniaturization of split rings using nanofabrication[56–58] led to the increase in the magnetic resonance frequency of metamaterials up to 100–300 THz (3–1 μm wavelength) may make near-field manipulating magnetic metamaterial devices feasible even in the visible region. The proposed model, generalized to the case of complex coupling constants due to retardation effects, may provide a useful tool for the design of such nanostructures with desirable guiding properties.

VI. CONCLUSIONS

A comprehensive theoretical and experimental study of dispersion properties of biatomic metamaterial structures, consisting of two coupled one-dimensional lines of metamaterial elements, each one capable of propagating a magnetoinductive wave, was presented. The anisotropy of the magnetic coupling between individual elements determined magnetic properties of these structures. The large variety of possible coupling arrangements allowed the tailoring of the dispersion curves for particular requirements. A general formulation in terms of coupling between any two nearest neighbors was set up. Modes of coupled guides supporting forward and/or backward waves with coupling strength dependent on the propagation constants were identified and the corresponding hybridization mechanisms for dispersion equations of magnetoinductive waves determined. Analytical predictions were verified both experimentally and numerically on a variety of coupled waveguides. The wavelength of magnetoinductive waves being much shorter than the free-space wavelength opens up the possibility of manipulating the near-field on a subwavelength scale. The approach can be employed for the design of near-field manipulating devices including a near-field magnetoinductive lens.

ACKNOWLEDGMENTS

The authors wish to thank Richard Syms for a number of stimulating discussions. Financial support of the DFG (GK 695 and Emmy Noether-Programme) is gratefully acknowledged by O.S., O.Z., and E.S. and that of the Royal Society (Incoming Visitor Scheme and International Joint Project Grant) by A.R., M.S., and C.J.S. M.S. is also supported by the Scheubeck-Jansen-Stiftung.

*Corresponding author. Email address: Ekaterina.Shamonina@uni-osnabrueck.de

[1] W. Rotman, IRE Trans. Antennas Propag. **10**, 82 (1962).
[2] W. Hardy and L. Whitehead, Rev. Sci. Instrum. **52**, 213 (1981).
[3] D. R. Smith, W. J. Padilla, D. C. Vier, S. C. Nemat-Nasser, and S. Schultz, Phys. Rev. Lett. **84**, 4184 (2000).
[4] V. G. Veselago, Sov. Phys. Usp. **10**, 509 (1968) [Usp. Fiz. Nauk **92**, 517 (1967)].
[5] R. A. Shelby, D. R. Smith, and S. Schultz, Science **292**, 77 (2001).
[6] J. B. Pendry, Phys. Rev. Lett. **85**, 3966 (2000).
[7] G. Atabekov, *Linear Network Theory* (Pergamon Press, Oxford, 1965).
[8] R. A. Silin and V. P. Sazonov, *Slow Wave Structures* (National Lending Library for Science and Technology, Boston SPA, England, 1971).
[9] G. H. Knittel, A. Hessel, and A. A. Oliner, Proc. IEEE **56**, 1822 (1968).
[10] M. Quinten, A. Leitner, J. Krenn, and F. Aussenegg, Opt. Lett. **23**, 1331 (1998).
[11] M. L. Brongersma, J. W. Hartman, and H. A. Atwater, Phys. Rev. B **62**, R16356 (2000).
[12] W. H. Weber and G. W. Ford, Phys. Rev. B **70**, 125429 (2004).
[13] S. A. Tretyakov and A. J. Viitanen, Electr. Eng. **82**, 353 (2000).
[14] N. Stefanou and A. Modinos, Phys. Rev. B **57**, 12127 (1998).
[15] A. Yariv, Y. Xu, R. K. Lee, and A. Scherer, Opt. Lett. **24**, 711 (1999).
[16] P. Thomas, M. Möller, R. Eichmann, T. Meier, T. Stroucken, and A. Knorr, Phys. Status Solidi B **230**, 25 (2002).
[17] P. Gay-Balmaz and O. J. F. Martin, J. Appl. Phys. **92**, 2929 (2002).
[18] E. Shamonina, V. A. Kalinin, K. H. Ringhofer, and L. Solymar, Electron. Lett. **38**, 371 (2002).
[19] E. Shamonina, V. A. Kalinin, K. H. Ringhofer, and L. Solymar, J. Appl. Phys. **92**, 6252 (2002).
[20] M. C. K. Wiltshire, E. Shamonina, I. R. Young, and L. Solymar, Electron. Lett. **39**, 215 (2003).
[21] M. C. K. Wiltshire, E. Shamonina, I. R. Young, and L. Solymar, J. Appl. Phys. **95**, 4488 (2004).
[22] A. Radkovskaya, M. Shamonin, C. J. Stevens, G. Faulkner, D. J. Edwards, E. Shamonina, and L. Solymar, J. Magn. Magn. Mater. **29**, 300 (2006).
[23] M. J. Freire, R. Marques, F. Medina, M. A. G. Laso, and F. Martin, Appl. Phys. Lett. **85**, 4439 (2004).
[24] M. J. Freire and R. Marques, Appl. Phys. Lett. **86**, 182505 (2005).
[25] I. S. Nefedov and S. A. Tretyakov, Microwave Opt. Technol. Lett. **45**, 98 (2005).
[26] R. R. A. Syms, E. Shamonina, and L. Solymar, IEE Proc., Part H: Microwaves, Antennas Propag. **152**, 77 (2005).
[27] O. Zhuromskyy, E. Shamonina, and L. Solymar, Opt. Express **13**, 9299 (2005).
[28] P. A. Belov and C. R. Simovski, Phys. Rev. E **72**, 036618 (2005).
[29] R. R. A. Syms, E. Shamonina, and L. Solymar, IEE Proc., Part H: Microwaves, Antennas Propag. **153**, 111 (2006).
[30] M. Beruete, F. Falkone, M. J. Freire, R. Marques, and J. D. Baena, Appl. Phys. Lett. **88**, 083503 (2006).
[31] O. Sydoruk, O. Zhuromskyy, E. Shamonina, and L. Solymar, Appl. Phys. Lett. **87**, 072501 (2005).
[32] A. Radkovskaya, O. Sydoruk, M. Shamonin, E. Shamonina, C. J. Stevens, G. Faulkner, D. J. Edwards, and L. Solymar (unpublished).
[33] M. C. K. Wiltshire, J. B. Pendry, I. R. Young, J. Larkman, D. J. Gilderdale, and J. V. Hajnal, Science **291**, 849 (2001).
[34] H. Chen, L. Ran, J. Huangfu, X. Zhang, K. Chen, T. Grzegorczyk, and J. A. Kong, J. Appl. Phys. **96**, 5338 (2004).
[35] A. J. Dekker, *Solid State Physics* (Macmillan, London, 1965).
[36] L. Lie, C. Caloz, C.-C. Chang, and T. Itoh, J. Appl. Phys. **92**, 5560 (2002).
[37] C. Caloz, A. Sanada, and T. Itoh, IEEE Trans. Microwave Theory Tech. **52**, 980 (2004).
[38] R. Ismal, F. Elek, and G. Eleftheriades, Electron. Lett. **40**, 315 (2004).
[39] Y. S. Tan, X. S. Rao, L. F. Chen, C. Y. Tan, and C. K. Ong, Microwave Opt. Technol. Lett. **45**, 255 (2005).
[40] G. Dolling, C. Enkrich, M. Wegener, J. F. Zhou, C. M. Soukoulis, and S. Linden, Opt. Lett. **30**, 3198 (2005).
[41] L. D. Landau and E. M. Lifschitz, *Electrodynamics of Continuous Media* (Pergamon Press, Oxford, 1984).
[42] L. Brillouin, *Wave Propagation in Periodic Structures* (Dover, New York, 1953).
[43] T. Tamir and A. A. Oliner, Proc. IEEE **110**, 310 (1963).
[44] A. S. Omar and K. F. Shünemann, IEEE Trans. Microwave Theory Tech. **33**, 1313 (1985).
[45] M. Mrozowski, *Guided Electromagnetic Waves: Properties and Analysis* (Research Studies Press, Hertfordshire, 1997).
[46] V. A. Kalinin and V. V. Shtykov, Sov. J. Commun. Technol. Electron. **36**, 96 (1991).
[47] M. Lapine, M. Gorkunov, and K. H. Ringhofer, Phys. Rev. E **67**, 065601(R) (2003).
[48] E. Shamonina, V. A. Kalinin, K. H. Ringhofer, and L. Solymar, Electron. Lett. **37**, 1243 (2001).
[49] R. Zengerle, J. Mod. Opt. **34**, 1589 (1987).
[50] D. R. Smith, D. Schurig, J. J. Mock, P. Kolinko, and P. Rye, Appl. Phys. Lett. **84**, 2244 (2004).
[51] R. A. Silin, *Periodic Waveguides* (Phasis, Moscow, 2002), in Russian.
[52] P. A. Belov, C. R. Simovski, and P. Ikonen, Phys. Rev. B **71**, 193105 (2005).
[53] M. C. K. Wiltshire, J. V. Hajnal, J. B. Pendry, D. J. Edwards, and C. J. Stevens, Opt. Express **11**, 709 (2003).
[54] M. C. K. Wiltshire, J. V. Hajnal, J. B. Pendry, and D. J. Edwards,

in *Proceedings of the 27th ESA Antenna Technology Workshop on Innovative Periodic Antennas: Electromagnetic Bandgap, Left-handed Materials, Fractal and Frequency Selective Surfaces, Santiago de Compostela, Spain, 2004* (ESA Publications Division, Noordwijk, The Netherlands, 2004).

[55] J. N. Gollub, D. R. Smith, D. C. Vier, T. Perram, and J. J. Mock, Phys. Rev. B **71**, 195402 (2005).

[56] S. Linden, C. Enkrich, M. Wegener, J. Zhou, T. Koschny, and C. M. Soukoulis, Science **306**, 1351 (2004).

[57] H. Schweizer, H. Gräbeldinger, T. Zentgraf, J. Kuhl, I. Loa, K. Syassen, and H. Giessen, in *Proceedings of the EPFL Latsis Symposium, Lausanne, Switzerland, 2005* (EPFL, Lausanne, 2005).

[58] M. W. Klein, C. Enkrich, M. Wegener, C. M. Soukoulis, and S. Linden, Opt. Lett. **31**, 1259 (2006).